Confocal imaging of the keratocyte network in porcine cornea using the fixable vital dye 5-chloromethylfluorescein diacetate

C. A. Poole[1], N. H. Brookes[2] and G. M. Clover[2]

Departments of [1]Anatomy and [2]Surgery, School of Medicine, University of Auckland, Auckland, New Zealand

Abstract

This study reports on the combined use of an aldehyde fixable, cell viability fluoroprobe, 5-chloromethylfluorescein diacetate (CMFDA), confocal laser scanning microscopy and digital image reconstruction, to produce high resolution images of corneal keratocyte preparations *in situ*. The central region of freshly enucleated porcine corneae were removed and stained overnight at 4°C with CMFDA. The tissue was washed, fixed, and frozen for cryosectioning in either a horizontal or antero-posterior orientation. Sections from anterior, central and posterior stroma were examined with a confocal microscope, and the digital images rendered as three-dimensional stereo reconstructions. Fluorescent CMFDA which completely permeated the cell bodies and extremes of the finest ramifying cell processes of all keratocytes provided exceptional high resolution images of the three morphologically distinct cell subpopulations at different levels of the stroma, and enabled improved characterisation of each cell type. Anteriorly was a thin, dense, non-lamellar network of keratocytes subjacent Bowman's membrane. In the central stroma, keratocytes were arranged in layers, the cell bodies had a flattened pyramidal or stellate shape, and the fine cell processes formed extensive distal ramifications. Immediately anterior to Descemet's membrane a small subpopulation of keratocytes with large cell bodies and short branched processes was identified. Extensive and diverse cell-to-cell contacts were orientated in all stromal planes, including ramping cell bridges between keratocyte lamellae in the central stroma. The use of the cell viability dye CMFDA is feasible and valuable for enhancing the visibility of entire keratocyte population in the intact cornea. Diverse multidirectional cell processes and intercellular contacts throughout the keratocyte network suggest a strong capacity for direct communication and cohesion in the maintenance and repair of the stromal matrix. Keratocytes closely related to the epithelium and endothelium have unique morphologies which may relate to specialised functions of these interface cells. Curr. Eye Res. 15: 165–174, 1996.

Correspondence: Dr. G. M. Clover, Ophthalmology Section, Department of Surgery, School of Medicine, University of Auckland, Private Bag 92019, Auckland, New Zealand

Key words: 5-chloromethylfluorescein diacetate; confocal microscopy; cornea; keratocytes; three dimensional reconstruction, pig

Introduction

The principal function of the keratocyte is the maintenance and repair of the corneal stroma. It is a highly modified cell with anatomical and physiological constraints specific to the requirements for corneal transparency. In the central stroma, the keratocyte cell body is currently perceived as attenuated, flattened and extensive, with cell processes projecting laterally between ordered arrays of collagen sheets termed lamellae. Until recently (1), no satisfactory investigation existed of comparative keratocyte morphology in the anterior, central and posterior stroma of the cornea.

Keratocyte distribution and transparency have rendered it difficult to investigate the precise microanatomy and intercellular connectivity of these cells throughout the cornea *in situ*. Whilst elucidative, early silver staining methods demonstrated gross keratocyte structure and connectivity (2), but were limited by the lack of resolution and difficulties in achieving a three-dimensional conceptualisation of keratocyte morphology. Subsequent scanning and transmission electron microscopy improved our understanding of keratocyte microanatomy (3–6), but were again limited by artefacts of matrix extraction and tissue processing, and the complexities of cellular reconstructions from multiple thin sections. Corneal keratocytes have also been visualised *in situ*, using a Tandem Scanning Confocal Microscope in reflection mode (7). While keratocyte morphology visualised using this method is consistent with previous reports, the limited resolution available with reflection confocal microscopy precludes detailed analysis of keratocyte morphology and heterogeneity. Recent studies, using immunohistochemical techniques coupled with Laser Scanning Confocal Microscopy to examine the keratocyte cytoskeleton (8), are also unable to visualise the keratocyte in its entirety, due to the specificity of the antibodies used.

In a recent study, we obtained significantly improved light

Received on July 25, 1995; accepted on October 12, 1995

microscopy images of the living keratocyte network *in situ* by using a cell viability fluoroprobe, Calcein-AM, to load the keratocyte cytoplasm (1). Calcein-AM freely permeates the cell membrane, where it reacts with the cytoplasmic esterases characteristic of viable cells to produce a polar molecule which fluoresces when excited by 488nm blue light. This dye enabled precise localisation of the keratocytes within the stroma, and three distinct subpopulations of keratocytes with differing morphology and orientation were identified in the anterior, central and posterior stroma (1). However, whilst Calcein-AM demonstrated the advantages of using cell viability probes to investigate keratocyte morphology, its application was limited by two important constraints. First, the viability of the preparation had to be maintained to prevent leaching of the dye, restricting the number of preparations which could be examined at any one time. Second, image resolution using light microscopy was limited by the need to examine fresh tissue dissections up to 500μm thick with minimum three dimensional conceptualisation of detailed cellular relationships and morphology.

In this study, we report the combined use of a new, aldehyde fixable, cell viability fluoroprobe, 5-chloromethylfluorescein diacetate (CMFDA), and confocal laser scanning microscopy to produce high resolution images of the keratocyte *ex vivo*. CMFDA is a glutathione-reactive dye which freely diffuses into the cytoplasm of viable cells, where it is catalysed by the ubiquitous enzyme glutathione S-transferase to produce a cell-impermeant, non-fluorescing product conjugated to glutathione and other thiol groups on intracellular proteins (9–10). In a separate reaction, intracellular esterases, common to most viable cells, cleave the acetate group from the conjugated dye molecule to produce a 'glutathione-fluorescent dye adduct' (9–10), spread throughout the entire cell cytoplasm. Hence CMFDA can only be loaded into living cells where the plasma membrane and intracellular biochemical reactions are maintained. Thus in functional cells, the dye diffuses throughout the extremities of the cytoplasm where it is immobilised by aldehyde fixation of cytoplasmic proteins.

This study demonstrates that the combination of cytoplasmic CMFDA staining and confocal image reconstruction provides superior visualisation of the orientation, the cytoplasmic microanatomy and interconnectivity of keratocyte cell bodies and ramifying cell processes which occupy the full depth of the corneal stroma. It illustrates in detail the three dimensional organisation of keratocyte subpopulations previously identified in our relatively low resolution light microscopic study of porcine corneas, and presents further morphological evidence for numerous 'ramping' cellular connections between adjacent keratocyte layers of the central corneal stroma.

Materials and methods

Tissue collection and CMFDA labelling

Experiments were performed using whole globes enucleated from freshly slaughtered pigs (3–5 months) obtained from the Auckland City Abattoir. These were stored at 4°C for transfer to the laboratory, where a central trephine (6mm in diameter) was taken from each cornea. This trephine was cut into two hemispheres and placed, epithelial side down, into separate wells of a 24-well multi-plate containing Cornea Transportation Media (CTM) (11) at 34°C, to ensure corneal maintenance under optimal conditions. This media consists of standard Cornea Organ Culture Medium supplemented with 5% Dextran (500,000 MW) to minimise swelling of the porcine corneae.

After 15 min equilibration, the media was aspirated from each well, and replaced with media containing 25μM CMFDA. The cornea were left to stain overnight in the dark at 4°C without agitation. This temperature was determined empirically to provide the optimum compromise between diffusion of CMFDA (which was significantly slower than Calcein-AM), discrete cytoplasmic labelling of all keratocytes, and minimum background staining (10). Following CMFDA loading, the stain solution was carefully aspirated, and the tissue gently washed three times with fresh media. The corneal samples were fixed in freshly prepared 2% paraformaldehyde for 10 min, and washed again with media. Each sample was equilibrated in an Epindorf tube containing media supplemented with 20% dimethyl sulphoxide (DMSO) which acts as a cryoprotectant, and frozen at −20°C for long term storage. For short term storage up to a maximum for 3 days, fixed corneae were immediately embedded in OCT compound (Tissue Tek, IN, USA), and prepared for cryosectioning.

To assess the effects of extended loading times, aldehyde fixation and freeze-thawing cryosectioning on keratocyte morphology, one fresh cornea was cut into 100μm thick lamellar slices using a Vibratome. These slices were stained with CMFDA for one h at 34°C to rapidly load the corneal tissue, washed with fresh media, mounted in a well slide, and examined immediately by confocal microscopy without further processing.

Cryosectioning

Prior to cryomicrotomy each corneal hemisphere was thawed and washed in media to remove residual DMSO. The tissue was frozen in OCT, great care being taken to ensure accurate anteroposterior or horizontal orientation. Cryosections 30μm thick were collected serially through the whole thickness of the cornea, and dried onto numbered slides. Representative sections from the anterior, central and posterior regions of the stroma were selected using conventional fluorescence microscopy, and mounted in VectaSheild (Vector Laboratories, CA, USA) for confocal imaging.

Confocal microscopy and image acquisition

Keratocytes were imaged using a Leica TCS 4d Confocal Laser Scanning Microscope (Leica, Heidelberg, Germany) equipped with a Leica DM RBE upright microscope, fitted with a motorised stage, transmitted and epi-illuminated light sources, a Krypton-Argon laser source and recommended filter sets, a range of infinity-adjusted optics for oil and water immersion, a transmitted light detector fitted with differential interference contrast optics, and dual channel photodetectors. To facilitate comparison with previous light microscopic studies using Calcein-AM (1), all sections were initially scanned using a Leica 40 × (NA = 1.0–0.5) infinity-adjusted oil immersion objective, and a series of single optical sections, 0.5μm thick, were collected

at 1μm intervals through the depth of the thick cryosection. These so-called *z*-series data sets therefore consist of 10–30 precisely paralell images collected through 10–30μm of the z axis. The imaging software (Leica Scanware) was used to select and enlarge (zoom) specific areas of interest within the field, which were scanned in more detail. To better define the interaction between fine keratocyte processes, a number of selected fields within each section were imaged at high magnification using Leica 63 × (NA = 1.4) and 100 × (NA = 1.3–0.6) infinity-adjusted oil immersion objectives. A z-series of 10–20 optical sections was collected and the scanning parameters for each image presented are included with each figure caption.

Digitised image data sets collected from the confocal microscope were transferred via an Ethernet link to a Silicon Graphics IRIS Indigo R4000 workstation with XS-24 graphics (Silicon Graphics, CA, USA), running Voxel View (Vital Images, CA, USA), a multifunctional image processing software package. Image data sets were stored on rewritable magneto-optical disks in a Parity magneto-optical disk drive, interfaced with the Silicon Graphics workstation.

All images were photographed using RX-100 black and white film (Agfa-Gevaert AG, Germany), either from high resolution monitors interfaced with both the confocal microscope and the Silicon Graphics workstation, or transferred (FTP) to an Apple Macintosh Centris computer, for imaging with an Agfa PCRII slide recorder (Agfa-Gevaert, Germany).

Image analysis

Image data sets, consisting of 10–30 perfectly parallel optical sections, were analysed with Leica Scanware and Voxel View, using several processing possibilities to construct the images presented. First, a *z*-series projection of all optical sections in the data set was constructed using Leica Scanware, producing a two dimensional image which was in perfect focus throughout the *z* axis. Second, Voxel View was used to construct a three dimensional representation of the entire data set, while 'projection lighting' was employed to create a surface rendered three dimensional object. Finally, the reconstructed image was rotated plus or minus 4 degrees about the *x* axis to produce stereo images of the keratocyte networks in different regions of the stroma.

Results

CMFDA labelling

Extended incubations at low temperature provided optimal dye loading conditions, producing brightly fluorescent keratocytes contrasted against the extracellular matrix which showed negligible background staining or autofluorescence. Qualitatively, no morphological differences were found between CMFDA loaded keratocytes imaged in fresh cornea, and those observed in fixed, frozen, cryosectioned tissue. This latter technique was chosen in preference since it provides for labelling of viable cells in an ex vivo state, allows aldehyde fixation and permanent preservation of morphologically identifiable cells, and permits serial sectioning and subsequent processing opportunities such as double labelling immunohistochemistry.

Anterior stroma

En face cryosections from the anterior stroma revealed a dense network of keratocytes immediately beneath Bowman's membrane (Fig. 1). The keratocyte cell bodies appeared flattened but irregular in shape, and branched extensively before terminating on adjacent cell bodies and cell processes (Fig. 1A). CMFDA staining was patchy in the cell bodies of some keratocytes, and was comparatively weak in the broad cell processes which dominated the anterior stromal matrix (Fig. 1B). A number of intensely stained intracellular particles were also observed within the cell body and cell processes of these anterior keratocytes (Fig. 1B).

Computer generated stereo reconstructions provided clear resolution of the three dimensional arrangement of cells within the anterior stroma, and must be examined with the aid of a stereo viewer (Figs. 1C-D, E-F). At lower magnifications (Figs. 1C-D), an extensive network of branching and interconnecting cell bodies and cell processes dominated the matrix, but showed a relatively poor lamellar organisation. Thus, while some overlapping and closely spaced cell bodies gave the appearance of vertical keratocyte 'stacks', the lateral and oblique projections of the broad cell processes creates a network of contacts throughout the anterior stroma (Figs. 1C-D).

At higher magnifications (Figs. 1E-F), stereo reconstructions demonstrated the flattened organisation but variable orientation of the cell bodies, and the high degree of interconnectivity between adjacent keratocytes. In addition, broad cytoplasmic projections created a three dimensional weave of overlapping, obliquely orientated cell processes which appear to form direct contacts with the cell bodies and processes of neighbouring keratocytes. None of the preparations examined showed evidence of keratocytes extending cell processes across Bowman's membrane to make direct contact with the basal cells of the epithelium.

Central stroma

Keratocytes in the central stroma stained intensely and uniformly with CMFDA, and while principally arranged in layers, the cell density was significantly lower than that of the anterior stroma at comparable magnifications (cf. Figs. 1A and 2A). Cell bodies had a flattened pyramidal or stellate shape, although this was not universal, and elongated keratocytes were regularly observed (Figs. 2A-B). Only occasionally could brightly fluorescent particles be identified intracellularly.

Staining of cell processes was less uniform than the cell bodies, but two distinct regions of a cell process could be identified. Proximally, the base was formed by thick, intensely stained 'stellate projections' which tapered from defined points around the cell body (Fig. 2B). Distally, these processes branched to form extremely fine cell processes which projected for considerable distances to achieve contact with neighbouring cell bodies and cell processes (Fig. 2B). Thus a key feature of dynamic cytoplasmic loading was the ability to identify extremely fine cell processes ($\leq 0.5\mu m$), and to trace their extensive distal ramifications over many microns.

Low powered stereo reconstructions from the central stroma provided further insights into general keratocyte morphology, including the variable orientation and inclination of the flattened cell

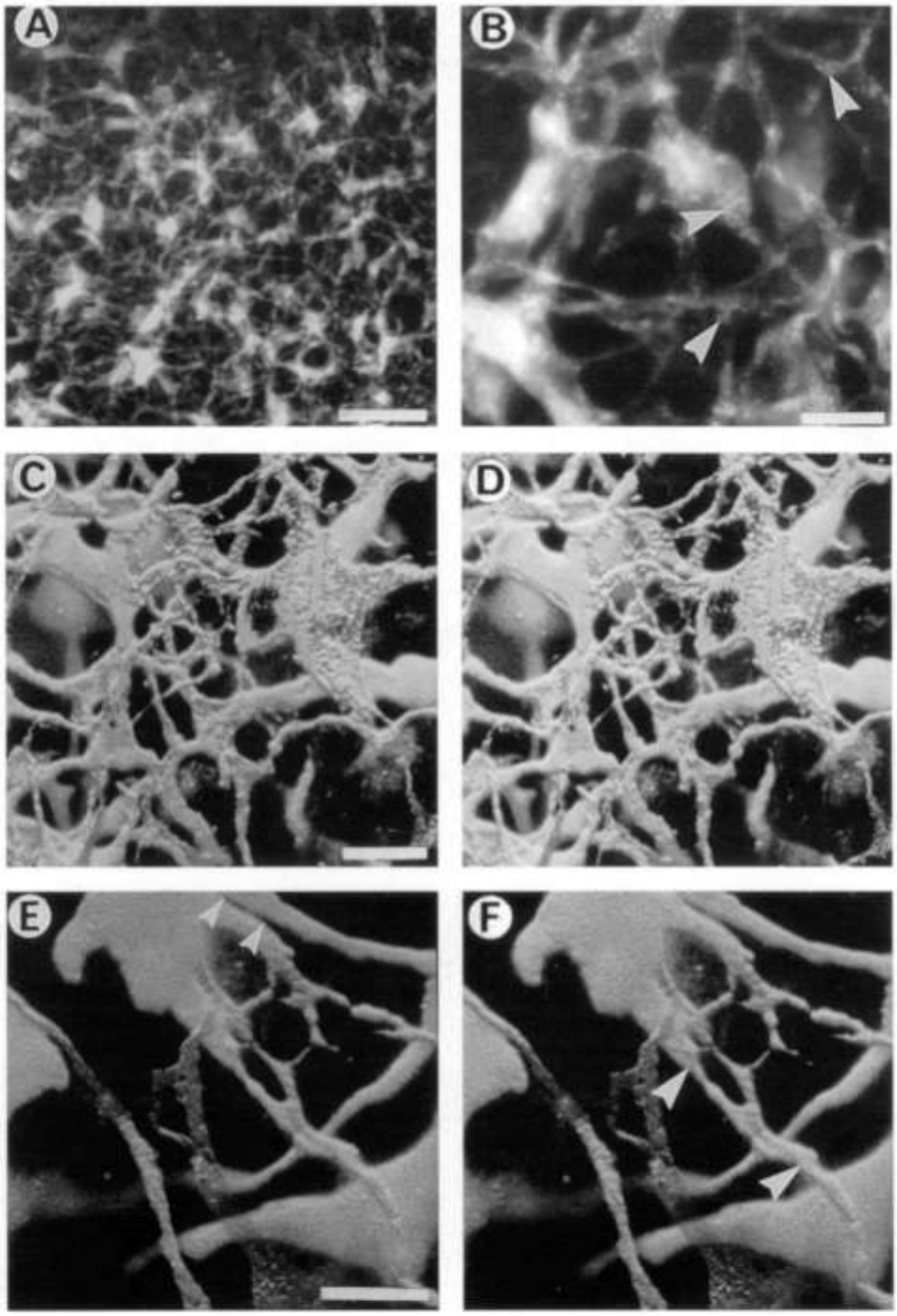

Figure 1. Anterior stromal keratocytes. (**A**) Standard low power projection showing the densely packed keratocytes and numerous cell processes which dominate this layer. (15 sections; 27.8μm z axis). Bar = 50μm. (**B**) Detailed z-series projection demonstrating patchy staining of cell bodies, reduced staining of thick cell processes, and the distribution of intensely stained intracellular organelles (arrows). (15 sections; 15.5μm z axis). Bar = 15μm. (**C** and **D**) Surface rendered stereo projection demonstrating the vertical stacking of cell bodies, and the profuse array of interwoven cell processes which traverse both x, y, and z axes. (13 sections; 13.6μm z axis). Bar = 20μm. (**E** and **F**) Detailed stereo projection showing the variable orientation of flattened cell bodies and the weave of cell processes projecting between them. A lateral contact has formed between a cell process and the margin of a cell body within the same plane (small arrows), while one process projects at an oblique angle through the reconstruction to interconnect keratocytes in adjacent planes of the section (large arrows). (14 sections; 7.5μm z axis). Bar = 10μm.

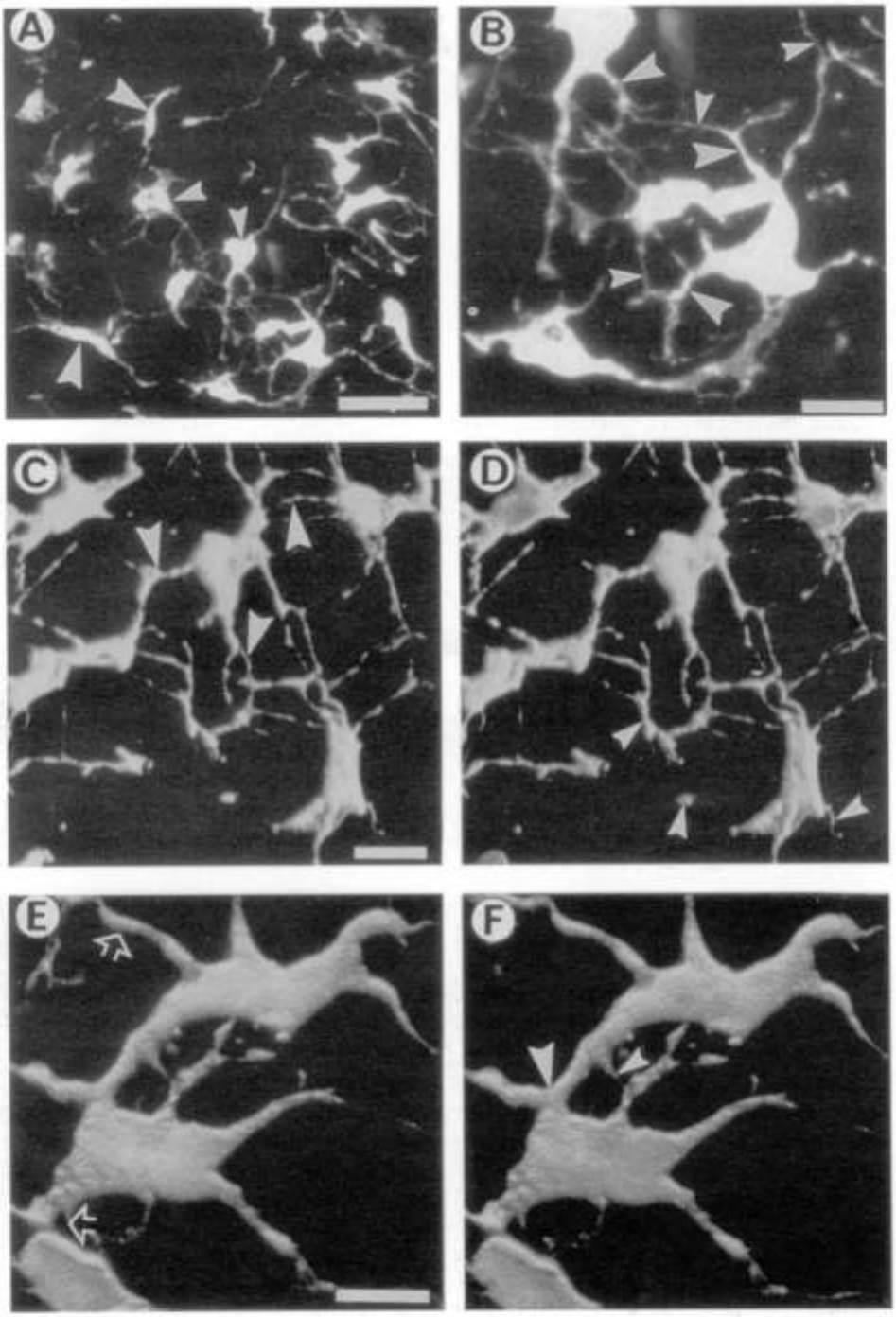

Figure 2. Central stromal keratocytes. (**A**) Standard z-series projection demonstrating flattened cell bodies with both stellate (small arrows) and elongate (large arrows) forms, and attenuated cell processes typical of mid stroma keratocytes. (18 sections; 18.9μm z axis). Bar = 50μm. (**B**) Detailed z-series projection from (**A**) showing the thick stellate projections which form the proximal base of most processes (large arrows), while the distal extremities branch and taper to form extremely fine cell processes (small arrows). (12 sections; 12.3μm z axis). Bar = 20μm. (**C** and **D**) Surface rendered stereo projection demonstrating the lateral interaction between cell processes and cell bodies. Processes with a curved, oblique trajectory through the reconstruction are highlighted (large arrows), while the profiles of cell bodies and cell processes aligned within the z axis are indicated by small arrows. (18 sections; 18.7μm z axis). Bar = 20μm. (**E** and **F**) High magnification stereo projection illustrating the thin flattened appearance of mid stromal keratocytes, the undulating contour of the cell bodies and the variable orientation of individual keratocytes. Cell processes project laterally, and obliquely in the z axis (open arrows), and were interconnected with adjacent keratocytes by cell process to cell process (small arrow) and cell process to cell body (large arrow) contacts. (10 sections; 9.4μm z axis). Bar = 10μm.

bodies, and the high degree of mutual interconnectivity between cell processes which extend up to 50μm between adjacent keratocytes (Figs. 2C-D). Moreover, careful scrutiny of these figures reveals a number of cell processes with curved oblique trajectories which intersect with keratocytes in different planes of the reconstruction. Indeed, some cell bodies and cell processes were orientated along the z axis, and therefore appeared as discrete, somewhat truncated structures which must be aligned at a tangent to the dominant orientation planar illustrated (Figs. 2C-D).

Since CMFDA diffuses throughout the cytoplasm, the entire volume of the keratocyte could be rendered at high magnification (Figs. 2E-F). Subtle curves and undulations were evident on the surface of most cell bodies, while the planar orientation and inclination of cell bodies appeared unique to each keratocyte (Figs. 2E-F). Notably, each cell process projecting from a keratocyte had a slightly different trajectory, extending laterally about the x-y axis, or obliquely through the z axis to intersect with the cell bodies and processes of keratocytes in adjacent lamellar planes (Figs. 2E-F).

The branching, layered arrangement of keratocytes in the central stroma is illustrated in Figures 3A-B, which is an antero-posterior stereo reconstruction of keratocytes viewed laterally. The twelve microns imaged in this reconstruction are an end-on view of only part of each keratocyte: the cells within one layer have a narrow network of processes which project laterally to interconnect adjacent cells within a particular plane. However careful examination of these reconstructions shows a significant number of cell bodies and their processes forming ramps from one cell layer to the next. These branching and obliquely orientated cell bodies and processes link layers such that there is a continuum of keratocytes throughout the corneal stroma (Figs. 3A-B).

Posterior stroma

Serial cryosectioning techniques allowed better characterisation of the distinct sub-population of keratocytes previously identified immediately anterior to Descemet's membrane (1). We confirmed the narrow range over which these cells could be identified (3–4 cells thick), care being taken to select and examine sections in which portions of the concave endothelium and Descemet's membrane could be accurately identified at the margins of the tissue.

Intense uniform staining was seen throughout keratocytes in this layer, while the cell density appeared greater than the central stroma, but less than the anterior stroma (cf. Figs. 1A, 2A and 4A). The cell bodies of posterior keratocytes appeared larger and more rounded than central stromal keratocytes, and were characterised by a significant increase in the number of short cell processes (Figs. 4A-B).

Computer generated stereo reconstructions confirmed the three dimensional interconnectivity between neighbouring keratocytes in the posterior stroma (Figs. 4C-D, 4E-F). Keratocyte cell bodies appeared large with a rounded contour, and were interconnected by short cell processes which projected laterally and obliquely to contact surrounding cell bodies or processes (Figs. 4C-D).

At higher magnifications (Figs. 4E-F), keratocytes in the narrow posterior layer had plump, undulating cell bodies and short thick cell processes forming contacts in the x, y and z axes. None of the preparations examined showed evidence of keratocytes extending cell processes across Descemet's membrane to make direct contact with the basal surface of the endothelial monolayer.

Discussion

This study employed the vital cell dye CMFDA (9–10), in combination with confocal laser scanning microscopy to produce high resolution three dimensional images of porcine keratocytes *in situ*. Whilst the results confirmed earlier studies on the presence of three morphologically distinct keratocyte sub-types in the corneal stroma of the porcine model (1), the current data provides unsurpassed images of keratocyte microanatomy and in particu-

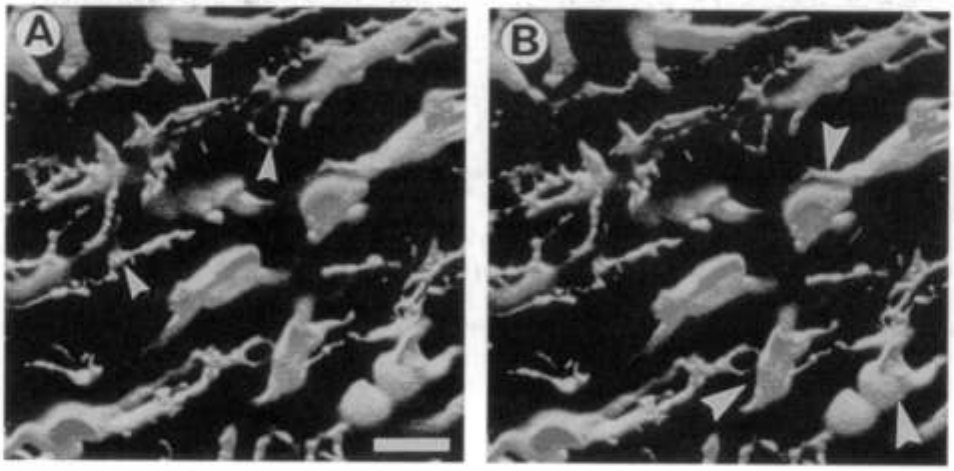

Figure 3. Central stromal keratocytes imaged from the side in an antero-posterior section. (**A** and **B**) Surface rendered stereo projection illustrating the lamellar organisation of cells in the central stroma, and the diversity of lateral connections between adjacent keratocytes within each plane (small arrows). Some cell bodies and processes form oblique ramping connections which interconnect cells in adjacent planes. (36 sections; 11.8μm z axis). Bar = 20μm.

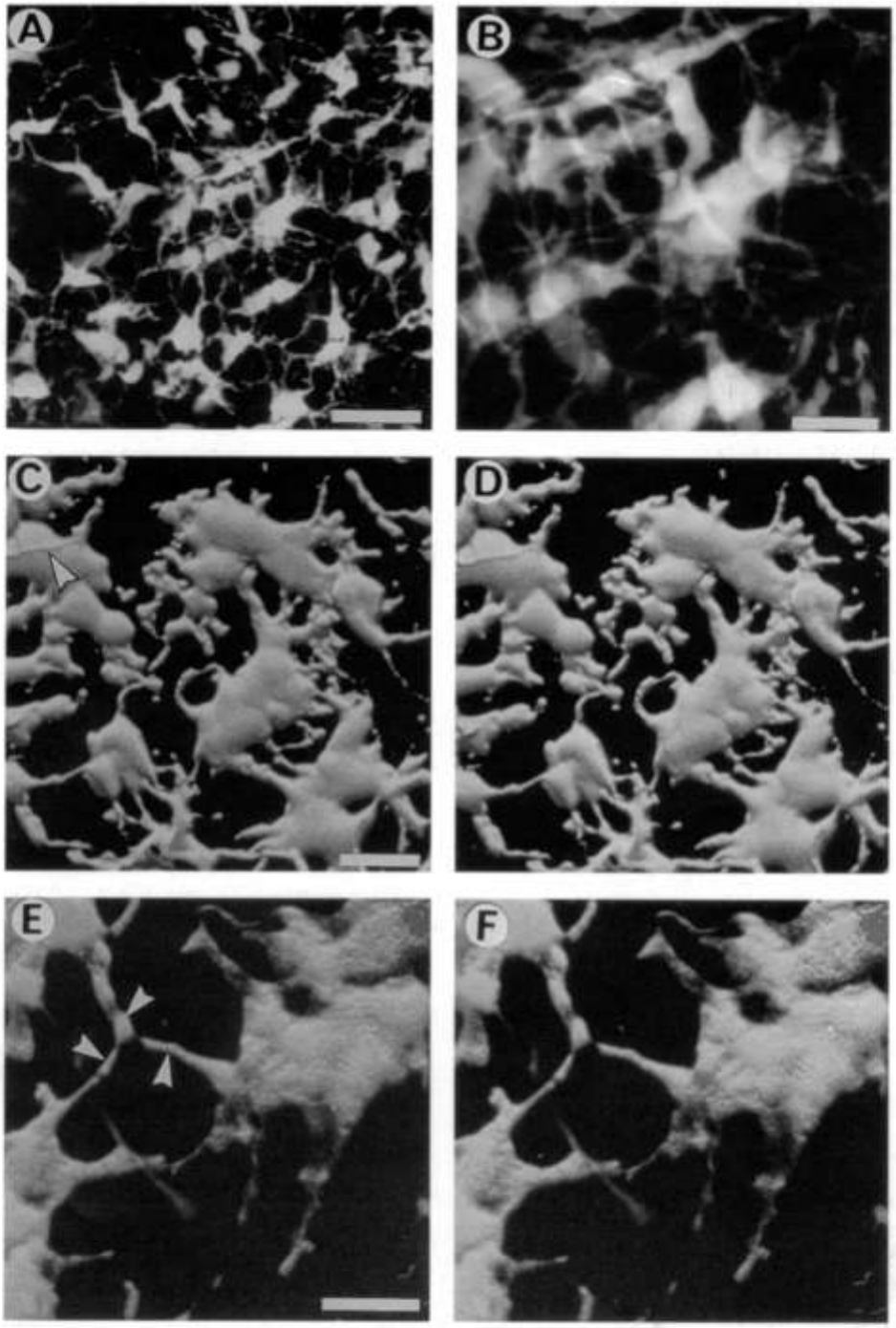

Figure 4. Posterior stromal keratocytes: (**A**) A standard z-series projection of the keratocytes immediately anterior to Descemet's membrane. Note increased keratocyte density, enlarge cell bodies and numerous short processes when compared to figure 2A. (16 sections; 16.7μm z axis). Bar = 50μm. (**B**) Detailed z-series projection from (**A**) showing large cell bodies and short cell processes continuous between adjacent keratocytes. (33 sections; 33.3μm z axis). Bar = 20μm. (**C** and **D**) Surface rendered stereo projection demonstrating the 'plump', rounded contour of cell bodies in the posterior stroma and the stumpy cell processes which project laterally and obliquely to contact neighbouring keratocytes in the x, y and z axes. A cell process in direct contact with a cell body is highlighted (arrow). (24 sections; 24.6μm z axis). Bar = 20μm. (**E** and **F**) Detailed stereo projection showing the fatter, undulating shape of the cell bodies, and the point of interaction between cell processes from three neighbouring keratocytes (small arrows). (10 sections; 10.0μm z axis). Bar = 10μm.

lar, more precise information on the three-dimensional organisation and interconnectivity of the stromal keratocyte network.

The use of CMFDA offers significant advantages over previous studies which employed fluorescein diacetate or Calcein-AM to elucidate keratocyte morphology in the corneal stroma (1). First, the nature of the dye reaction, involving as it does both intracellular glutathione S-transferase and esterase enzymes, ensures the fluoroprobe is complexed to the exposed glutathione residues of intracellular proteins (9–10). These reactions provided permanent anchoring of the dye and markedly improved dye retention when compared with Calcein-AM. Secondly, the ubiquitous distribution of glutathione S-transferase and esterase ensure CMFDA was dispersed throughout the cytoplasm, permitting complete visualisation of the entire cell cytoplasm rather than specific immunohistochemical identification of just one intracellular component such as actin (8). Third, due to its complexing reaction with intracellular proteins, CMFDA staining could be made 'permanent' by protein fixation with aldehydes, preferably paraformaldehyde, which minimised autofluorescence in the specimen. Finally, fixed tissue prepared by cryomicrotomy or vibratome sectioning allowed accurate selection of cells from each layer of the stroma, and provided the thick sections (25–50μm) necessary to optimise the optical z-sectioning capabilities of the confocal microscope which has not previously been reported in studies of this type.

The major disadvantage of CMFDA staining was its rate of penetration through the dense stromal matrix, being considerably slower than Calcein-AM or fluorescein diacetate used in a previous study (1). Extended loading periods at low temperature provided a satisfactory compromise for optimal staining (10), producing enhanced contrast between the labelled keratocytes and the extracellular matrix which showed negligible background staining. Qualitatively, there were no apparent morphological differences between keratocytes imaged in fresh vibratome sectioned corneae, and those observed in fixed, cryosectioned material. This latter technique was chosen in preference, since it provided permanent preservation of the specimens and further downstream processing opportunities. This CMFDA loading protocol, in combination with high resolution confocal microscopy, provided superior images to those previously published using Calcein-AM (1), and convincingly establish the heterogeneity of keratocytes in the porcine corneal stroma.

This study was confined to the optically important zone of the cornea, and no attempt was made to establish either qualitative or quantitative differences between the central and peripheral regions of the cornea. Of the three distinct keratocyte sub-populations identified in the optical zone, two were closely related to the metabolically active epithelial and endothelial cell layers. No keratocytes or their cell processes were observed to traverse either Bowman's or Descemet's membranes, implying that no direct contacts exist between the stromal keratocytes and the basal aspects of the corneal interface layers. Moreover, the dense random arrangement of keratocytes in the anterior stroma close to Bowman's membrane does not appear to preclude transparency, an observation which equally applies to the relatively narrow layer of bulky posterior keratocytes subjacent to Descemet's membrane. The topography of these two keratocyte sub-populations is probably not related solely to the differing orientations of the collagen fibrils in those regions (12). Rather, their morphological differences may be related to functional specialisations and interactions due particularly to their position and potential role as interface keratocytes between the bulk of the stroma and the effects of normal activity, or dysfunction of the epithelial and endothelial cell layers.

Previous authors have reported findings unique to anterior keratocytes such as increased nuclear density (13), mitochondrial density (14), differences in the lectin binding properties (15), and altered responses to epithelial loss (16–18). In the present study, intensely fluorescent intracellular particles were common in keratocytes from the anterior stroma, but became less prominent in the central and posterior stroma. While the possibility exists that these particles may be intracellular vesicles containing CMFDA, their regular size, cylindrical shape, and clustered distribution in the cell body, suggests they may also be mitochondria which have selectively concentrated the dye. Furthermore, de-epithelialisation has recently been shown to initiate epithelial-induced, cytokine-mediated, sub-epithelial keratocyte apoptosis (17), indicating the presence of cytokine-specific receptors within anterior keratocytes. Thus the specific functions of the anterior stroma and its unique keratocytes requires continued investigation, particularly at this time when excimer laser photorefractive keratectomy and the mechanisms responsible for the induced stromal remodelling have yet to be fully elucidated.

However, the structurally specific posterior keratocytes identified in this study only occupy a very narrow band immediately anterior to Descemet's membrane, and do not correlate with Neuronal-specific Enolase distribution described in the posterior one-third of the stroma and endothelium (19).

The keratocyte sub-type which formed the major cellular component of the stroma was characterised by irregularly shaped, flattened cell bodies and substantially longer cell processes which project laterally and obliquely to contact keratocytes in the same and adjacent planes of the stroma. As indicated by Hogan (4), this dominant keratocyte sub-type appears specifically designed to fulfil a function in maintaining the majority of the corneal stroma, but with morphological constraints to conserve transparency throughout the considerable tissue thickness of the central stromal region.

An important feature to emerge from this study was the imaging of extremely fine cell processes which project from central stromal keratocytes. Whilst fine processes have previously been identified by conventional light and transmission electron microscopy (2–5), these techniques are limited by resolution or the need for extensive serial thin section reconstructions, and have not fully displayed the complexity of these extremely fine, very attenuated, multi-directional cell processes. Scanning electron microscopy has also failed to elucidate these structures since this method generally requires enzymatic digestion of the collagenous matrix (6), treatments which are likely to introduce significant distortions in the fine structure of the keratocyte network. Thus the combination of the vital cytoplasmic dye CMFDA, confocal microscopy and three-dimensional image reconstruction have provided exceptionally high resolution images of the keratocyte network *ex vivo*, and should improve interpre-

tation of the images obtained using Tandem Scanning Confocal Microscopy in the clinical environment (7).

Surfaced rendered stereo projections provided additional information on the three dimensional organisation of stromal keratocytes and the projection of their cell processes. While two dimensional lateral cellular contacts have previously been thought to dominate in the central stroma, the current study has shown that some cell bodies and processes extend between the planes of keratocytes to form cellular 'ramps', or obliquely orientated cellular bridges which link central stromal keratocytes in different horizontal planes. Cellular 'ramps' are best illustrated in the stereo reconstructions of antero-posterior sections (Fig. 3), and while confirming our earlier light microscopic observations (1), the current study has revealed these 'ramps' to be quite numerous, with diverse orientations of the cell bodies and processes involved. Thus cellular 'ramps' could provide the anatomical substructure necessary for widespread antero-posterior intercellular communication which has previously been presumed to be minimal since cell bodies or processes extending between adjacent keratocyte planes were infrequently identified. This study suggests that keratocytes should no longer be considered to have predominantly lateral cell process contacts.

In summary, the use of CMFDA to visualise viable keratocytes in intact porcine corneae, coupled with serial optical sectioning by confocal microscopy and image reconstruction, has resulted in high resolution three dimensional images of keratocyte morphology not previously achieved. This data confirms the presence of three distinct keratocyte sub-populations in the porcine corneae and provides new information on their micro-anatomical characteristics and orientation. It was evident that all cells which comprise these newly identified layers formed extensive interconnections in three dimensions, but the precise sites and nature of these cell contacts have yet to be fully identified. The detailed structural analysis presented in this study suggests these contacts could include cell process-to-cell process, cell process-to cell body, and possibly cell body-to-cell body interactions. This study therefore highlights the extraordinary potential for far-reaching, three-dimensional cellular connectivity within all layers of the keratocyte network. It is an observation which is in agreement with recently emerging experimental evidence that keratocytes networks show potential for dynamic and cohesive responsiveness to stromal as well as epithelial and endothelial-generated cytokines (20–22).

Acknowledgements

This research was supported (in part) by the Health Research Council of New Zealand (CAP), The Maurice and Phyllis Paykel Trust and The New Zealand National Eye Bank (NHB/GMC), and The Sir William and Lady Stevenson Trust (GMC).

References

1. Poole, C. A., Brookes, N. H. and Clover, G. M. (1993) Keratocyte networks visualised in the living cornea using vital dyes. *J. Cell Sci.* **106**, 685–692.
2. Sverdlick, J. (1954) Study of keratocytes by means of del Rio Hortega's method of silver impregnation. *Acta XVII Int. Cong. Ophthal.* **3**, 1887.
3. Scharenberg, K. (1955) The cells and nerves of the human cornea. *Am. J. Ophthal.* **40**, 368–279.
4. Hogan, M. J., Alvarado, J. A. and Weddell, J. E. (1971) *Histology of the Human Eye.* W. B. Saunders, London, UK.
5. Marshall, J. and Grindle, C. F. J. (1978) Fine structure of the cornea and its development. *Trans. Ophthalmol. Soc. UK.* **98**, 320–328.
6. Nishida, T., Yasumoto, K., Otori, T. and Desaki, J. (1988) The network structure of corneal fibroblasts in the rat as revealed by scanning electron microscopy. *Invest. Ophthalmol. Vis. Sci.* **29**, 1887–1890.
7. Petroll, W. M., Jester, J. V. and Cavanagh, H. D. (1994) In vivo confocal imaging: general principles and applications. *Scanning*, **16**, 131–149.
8. Jester, J. V., Barry, P. A., Lind, G. J., Petroll, W. M., Garana, R. and Cavanagh, H. D. (1994) Corneal keratocytes: *in situ* and *in vitro* organisation of cytoskeletal contractile proteins. *Invest. Ophthalmol. Vis. Sci.* **35**, 730–743.
9. Haugland, R. P. (1992) Handbook of fluorescent probes and research chemicals. Molecular Probes, Oregon.
10. Poole, C. A., Brookes, N. H., Gilbert, R. T., Beaumont, B. W., Crowther, A., Scott, L. and Merrilees, M. J. (1995) Detection of viable and non-viable cells in connective tissue explants using the fixable fluoroprobes 5-chloromethyl-fluorescein diacetate and ethidium homodimer-1. *Conn. Tiss. Res.* In press.
11. Armitage, W. J. and Moss, S. J. (1990) Storage of corneas for transplantation. In *Current Ophthalmic Surgery* (Ed. Easty, D. L.). Pp. 193–199. Baillère Tindal, London, UK.
12. Birk, D. E. and Trelstad, R. L. (1984) Extracellular compartments in matrix morphogenesis: collagen fibril, bundle, and lamellar formation by corneal fibroblasts. *J. Cell Biol.* **99**, 2024–2033.
13. Petroll, W. M., Boettcher, K., Barry, P., Cavanagh, H. D. and Jester, J. V. (1995) Quantitative assessment of antero-posterior keratocyte density in the normal rabbit cornea. *Cornea*, **14**, 3–9.
14. Stockwell, R. A. (1991) Morphometry of cytoplasmic components of mammalian articular chondrocytes and corneal keratocytes: species and zonal variations of mitochondria in relation to nutrition. *J. Anat.* **175**, 251–261.
15. Schanzlin, D. J., Kratz-Owens, K. and Hageman, G. S. (1990) Keratocyte subpopulation as revealed by lectin-binding. *Invest. Ophthalmol. Vis. Sci.* **31**, **32**.
16. Szerenyi, K. D., Wang, X., Gabrielian, K. and McDonnell, P. J. (1994) Keratocyte loss and repopulation of anterior corneal stroma after de-epithelialization. *Arch Ophthalmol.* **112**, 973–976.
17. Ishizaki, K., Arar, H., Wander, A. H. and Kao, W. W.-Y. (1995) Apoptosis during corneal wound-healing. Invest. *Ophthalmol. Vis. Sci.* **36**, S867.
18. Essepian, J. P., Rajpal, R. K., Azar, D. T., New, K., Antonacci, R., Sheilds, W. and Stark, W. J. (1994) The use of confocal microscopy in evaluating corneal wound healing after excimer laser keratectomy. *Scanning* **16**, 300–304.

19. Adamis, A. P., Molnar, M. L., Tripathi, B. J., Emmerson, M. S., Stefansson, K. and Tripathi R. C. (1985) Neuronal-specific enolase in human corneal endothelium and posterior keratocytes. *Exp. Eye Res.* **41**, 665–668.
20. Fabre, E.J., Bureau, Y., Pouliquen, Y. and Lorans, G. (1991) Binding sites for human interleukin-1 alpha interferon, and tumour necrosis factor on cultured fibroblasts of normal cornea and keratoconus. *Curr. Eye Res.* **10**, 585–592.
21. Wilson, S. E., He, Y.-G., Weng, J., Li, Q., Vital, M. and Chwang, E. L. (1995) Epithelial- and endothelial-derived interleukin-1 (IL-1) modulates corneal tissue organisation and wound healing response through induction of keratocyte apoptosis. Invest. *Ophthalmol. Vis. Sci.* **36**, S866.
22. Masur, S. K., Erenburg, I., Dinh, T. T., Connors, R. Jr. and Dewal, H. S. (1995) TGF-beta secretion induces myofibroblast differentiation in cultured corneal fibroblasts. Invest. *Ophthalmol. Vis. Sci.* **36**, S867.